Automated Detection of Proliferative Diabetic Retinopathy using a Modified Line Operator and Dual Classification

R.A. Welikala[a,*], J. Dehmeshki[a], A. Hoppe[a], V. Tah[b], S. Mann[c], T.H. Williamson[c], S.A. Barman[a]

[a] Digital Imaging Research Centre, Faculty of Science, Engineering and Computing, Kingston University, London, United Kingdom.

[b] Medical Retina, Oxford Eye Hospital, Oxford, United Kingdom.

[c] Ophthalmology Department, St Thomas' Hospital, London, United Kingdom.

[*] Corresponding author. Tel.: +44 7944990065. E-mail address: Roshan.Welikala@kingston.ac.uk (R.A. Welikala).

Abstract:

Proliferative diabetic retinopathy (PDR) is a condition that carries a high risk of severe visual impairment. The hallmark of PDR is neovascularisation, the growth of abnormal new vessels. This paper describes an automated method for the detection of new vessels in retinal images. Two vessel segmentation approaches are applied, using the standard line operator and a novel modified line operator. The latter is designed to reduce false responses to non-vessel edges. Both generated binary vessel maps hold vital information which must be processed separately. This is achieved with a dual classification system. Local morphology features are measured from each binary vessel map to produce two separate feature sets. Independent classification

is performed for each feature set using a support vector machine (SVM) classifier. The system then combines these individual classification outcomes to produce a final decision. Sensitivity and specificity results using a dataset of 60 images are 0.862 and 0.944 respectively on a per patch basis and 1.00 and 0.90 respectively on a per image basis.

1 INTRODUCTION:

Diabetes is a disorder of sugar metabolism and is characterized by raised levels of glucose in the blood. These high levels can damage the vessels that supply blood to vital organs. Diabetic retinopathy (DR) is the resultant condition affecting the retinal vasculature, leading to progressive retinal damage that can end in loss to vision and blindness [1]. DR is recognized as the leading cause of blindness in the working-age population [2]. The problem is increasing in its scale, with diabetes having been identified as a significant growing global public health problem [3]. 171 million people were estimated to have diabetes worldwide in the year 2000 and this figure is expected to rise to 366 million by the year 2030 [4].

The purpose of DR screening is to detect potentially sight threatening disease at an early stage which is when treatment and management is the most effective [5,6]. In the United Kingdom diabetic patients aged 12 and above are invited, at least annually, for a screening appointment where retinal images are captured using digital photography [7]. With such a large diabetic population, assessment of these images can be a time consuming and costly task. Therefore the introduction of automated detection systems would be greatly beneficial to this field [8].

The damage to the retinal blood vessels will cause blood and fluid to leak on the retina and form features such as microaneurysms, haemorrhages, exudates, cotton wool spots and venous loops [9]. With progression, the blockages and damage to blood vessels will cause areas of retinal ischaemia to develop and in an attempt of revascularization the growth of new blood vessels is triggered. The growth of new vessels represent the advanced stages of DR known as proliferative diabetic retinopathy (PDR), which poses a high risk of severe vision loss due to the fragile nature of the new vessels making them prone to bleed and cause pre-retinal and vitreous haemorrhages. Also fibrous tissue gradually develops in association as new vessels increase in size and this can cause tractional retinal detachment [10]. Patients presenting PDR require an urgent referral to a specialist.

Whilst disease/no disease automated grading system do provide benefits [11], an additional aim is to develop a system capable of triaging images. This should include the ability to detect and prioritise PDR images to ensure immediate attention and treatment. The automatic detection of DR has received a lot of research attention, with studies investigating microaneurysm and haemorrhage detection [12-16], and exudate detection [17-21]. In contrast, little work has been done to detect PDR.

New vessels are termed according their location, new vessels at the optic disc (NVD) and new vessels elsewhere (NVE). They appear as unregulated vessel growth, initially appearing as loops or networks that appear on the optic disc or near a vein. As they grow they form dense lacy networks which usually pass across the underlying veins and arteries. They tend to be fine in calibre and are more tortuous and convoluted than normal vessels. New vessels tend to grow away from the retinal surface and hence can appear out of the focal plane of the photograph, which can result in a blurry and obscure appearance. A retinal image containing new vessels is shown in figure 1(a).

Vessel segmentation is often the first step of new vessel detection methods, with the purpose of analysing the morphology of the binary vessel map in search of abnormality. Vessel segmentation has received the largest share of attention in the field of retinal image analysis, studies include [22-29]. Segmentation techniques often proceed into methodologies that classify vessels as arteries or veins and measure vessel calibre [30,31] for application in cardiovascular disease studies. A comprehensive review of this mature field of vessel segmentation is provided by Fraz [32]. However these techniques struggle with segmenting new vessels due to their irregular appearance.

The following vessel segmentation techniques were designed with new vessels taken into consideration. L.Zhang [33] proposed a modified matched filter that used double sided thresholding. The main emphasis was not on the increased segmentation of new vessels, but instead the reduction of the false response to exudates which can cause large local densities on the segmented map and therefore can be mistaken for new vessels. B.Zhang [34] applied the matched filter with the first-order derivative of the Gaussian to reduce the false response to exudates. Figure 1(b) shows a retinal image with exudates, also known as bright lesions. Ramlugun [35] described a small vessel extraction technique, the main contribution was the varying of the clip limit for contrast limited adaptive histogram equalization (CLAHE) to allow more contrast for small vessels.

The following new vessel detection methods applied vessel segmentation prior to the described analysis methods. Daxer [36] and Karperien [37] both described the retinal vasculature as a fractal and used the fractal dimension to quantify its complexity to indicate the presence of new vessel growth. Jelinek [38] extracted morphological features based on data obtained from the application of the derivatives of Gaussian wavelets to the vessel skeleton. Goatman [39] developed a comprehensive set of 15 features including the number of vessel segments, the mean vessel wall gradient and various tortuosity measures to detect

new vessels on the optic disc. Akram [40] proposed a Gaussian mixture model based classifier with a 5 dimensional feature set based on intensity and gradient values. Hassan [41] used just two local features, the number of vessels and the area of vessels within a small scanning sub-window to indicate new vessels. In [42], the majority of normal vasculature was removed from the vessel map to simplify new vessel detection.

The next described methods do not perform vessel segmentation and therefore avoid the difficulties associated with segmenting new vessels. Statistical texture measures calculated using the grey level co-occurrence matrix (GLCM) were applied by Frame [43] to identify irregular distributions of pixel intensities associated with neovascularisation. Acharya [44] calculated texture features from the GLCM and the run length matrix to identify the stage of DR. Agurto [45] utilised multi-scale amplitude modulation frequency modulation (AM-FM) methods for spectral texture analysis to characterise different retinal structures, including new vessels. However, later work by Agurto [46] involved AM-FM along with granulometry and vessel segmentation to detect new vessels on the optic disc.

There exist techniques developed from other research topics that are very relevant to PDR detection. Zutis [47] presented a system using edge contour analysis for detecting abnormal retinal capillary regions, with the focus on telangiectasia. Doukas [48] created an automated method for the quantification of micro-vessel density within the inner surface of egg shells in order to study the angiogenesis in developing chick embryos. Measures included vessel length, branching points and GLCM textural information.

The main contribution of the proposed method is the novel application of a dual classification approach to independently process the binary maps from two different vessel segmentation methods with the aim to detect new vessels and reduce false responses caused by other retinal features. This includes a novel modified line operator, based on double sided thresholding, designed to segment vessels whilst reducing false responses to non-vessel edges.

The organization of this paper is as follows. Section 2 describes details of the methodology.

Section 3 presents the experimental evaluation. Finally, a discussion and conclusion is given in

section 4.
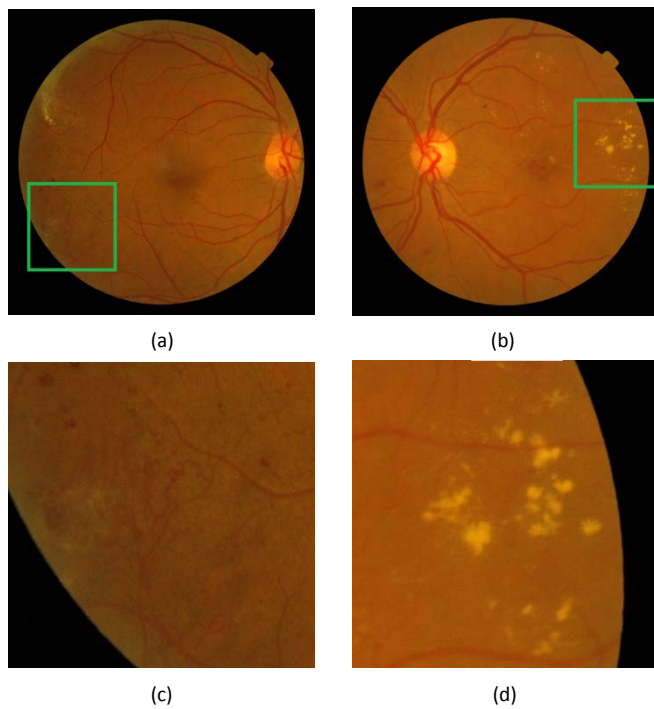
Fig. 1: (a) Retinal image with new vessels. (b) Retinal image with bright lesions. (c)-(d) Zoom-in

images of (a)-(b).

2 METHODOLOGY:

The proposed dual classification system was adapted from the general preferred approach of

the use of vessel segmentation followed by analysis of the binary vessel map to detect new

vessels. The architecture of this system is shown is figure 2. Initial steps included spatial

normalization to ensure the system's robustness with respect to image resolution and pre-

processing to enhance the vasculature. Thereafter the system splits into two pathways as two different vessel segmentation methods were applied to create two binary vessel maps. Each map held vital information and it was important that they were processed separately. The two segmentation methods used were the standard line operator approach and a novel modified line operator approach. The latter was designed to reduce false responses to non-vessel edges. Straight vessel removal was applied to remove large sections of normal vasculature from the binary vessel maps. Structural analysis was applied to the resultant where local features associated with the morphology of the vasculature were measured. Each pathway had its own feature set produced, using the same set of local features. Independent classification was performed for each feature set using a linear support vector machine. The system produced a final decision by combining the two individual classification outcomes in which regions of the retina were labelled as new vessels or non-new vessels. The main purpose of the novel application of a dual classification system in retinal image analysis is to detect new vessels whilst reducing false responses caused by other common retinal features.
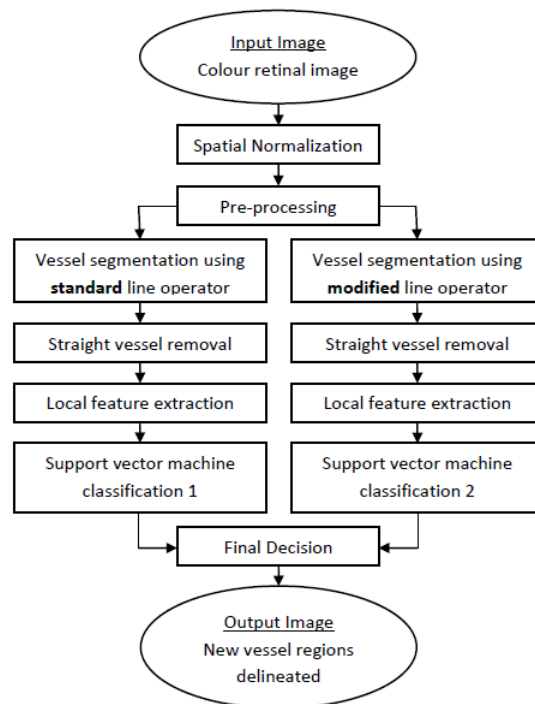
Figure 2: System architecture.

2.1 Pre-processing:

Retinal images often show light variations, poor contrast and noise. This, along with the fact that new vessels tend to lack distinction meant that pre-processing was required. The green channel exhibits the best vessel/background contrast while the red and blue tend to be very noisy. Therefore the inverted green colour channel was used, where vessels appear brighter than the background. A median filter was applied to reduce salt and pepper noise. Local contrast enhancement was achieved by applying contrast limited adaptive histogram equalisation (CLAHE) [49]. Shade correction was performed by subtracting an image approximating the background. This approximation was obtained by applying a median filter with a 105 x 105 pixel size kernel. This large size was chosen to ensure new vessel regions

were preserved. A morphological top-hat transformation was used to produce an image containing small circular objects (microaneurysms) [12] which were then subtracted from the image. A pre-processed image is shown in figure 3, which has been inverted back again only for better visualisation.
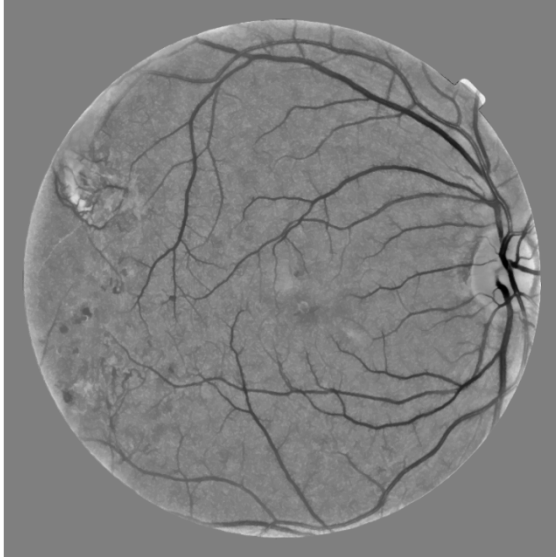
Figure 3: Pre-processed version of figure 1(a).

2.2 Line Operator /Modified Line Operator:

The detection of linear structures has become a topic of significant importance in medical image analysis mainly due to the fact that vessels can be approximated as being piecewise linear. Ricci [27] applied line operators to detect linear structures in retinal images having been inspired by a method [50] which applied a line operator to detect linear structures in mammographic images.
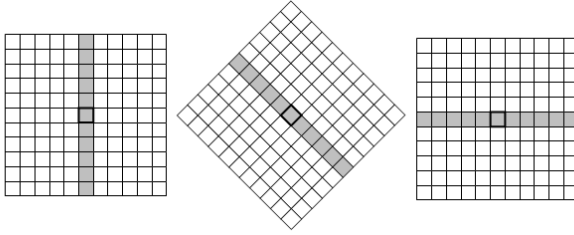
Figure 4: Standard line operator at 3 different orientations.

The standard line operator is illustrated in figure 4. The average grey-level of the pixels lying on a line passing through the target pixel (i,j) was calculated for multiple orientations. The orientation giving the largest value was found and its value was denoted with $\mathbf{L}(i,j)$. The line strength of the pixel, $\mathbf{S_1}(i,j)$, is given by

$$\mathbf{S_1}(i,j) = \mathbf{L}(i,j) - \mathbf{N}(i,j) \qquad\qquad (1)$$

where $\mathbf{N}(i,j)$ is the average grey-level of the similarly orientated neighbourhood. Conversely to [27], the whole window was orientated as opposed to keeping a fixed window and orientating only the line. At certain orientations, the line's path could not be exactly matched by the pixel grid, thus line and region averages were found by using nearest neighbour interpolation instead of bi-linear interpolation.

The line strength was large if the winning line was aligned with a vessel. In figure 5, the line strength images corresponding to the images in figure 1 are shown. The parameters were selected to ensure an adequate response to new vessels was achieved. The line operator of length 15 pixels and width 25 pixels was applied over 12 different orientations (angular resolution of 15°). The square dimensions of the line operator did not have to be adhered to, the operator width was selected in accordance to vessel width and the operator length was selected to be relatively short as new vessels tend to be tortuous. An empirically derived threshold, T1, was applied to the line strength image to produce segmentation of the vessels. T1 was chosen to be relatively low to ensure that faint and obscure new vessel segments were

retained. Figure 6 shows the binary vessel maps corresponding to the images in figure 1. The new vessels had been segmented with reasonably accuracy, thus meaning their properties could be adequately analysed. Considering some simple properties of new vessels such as high local density and large curvatures, it is evident from figure 6 that new vessels were distinguishable to normal vasculature.

(a) (b)

(c) (d)
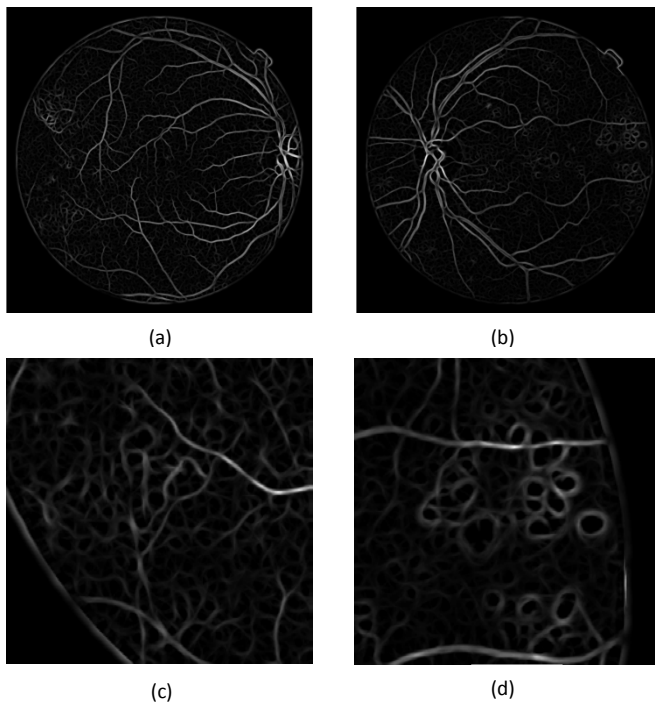
Figure 5: Line strength maps corresponding to the images in figure 1.

(a)

(b)

(c)

(d)
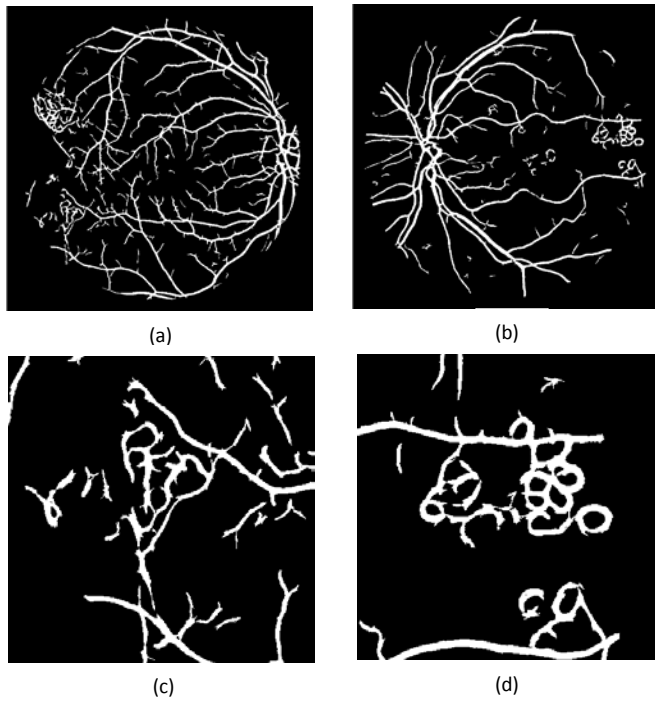
Figure 6: Binary vessel maps corresponding to the images in figure 1, standard line operator.

A well documented problem of vessel segmentation is that they respond not only to vessels but also to non-vessel edges. Bright lesions cause the most misclassifications. Areas of glare or reflection artefact, which are common on retinal images of younger individuals, also cause false responses. Figure 5 illustrates the strong line strength response to vessels as well as the edges of the bright lesions and figure 6 shows that after thresholding both the vessels and the edges of the bright lesions were detected. These false detections caused large local densities and large curvatures which were undistinguishable to new vessels.

A novel modified line operator was developed to reduce the false responses to non-vessel edges, inspired by L.Zhang [33] where a matched filter with double sided thresholding was proposed. Three modified line strength measures were derived,

$$S_2(i,j) = L(i,j) - N_R(i,j) \qquad (2)$$

$$S_3(i,j) = L(i,j) - N_L(i,j) \qquad\qquad (3)$$

$$S_4(i,j) = L(i,j) - N_B(i,j) \qquad\qquad (4)$$

where $N_R(i,j)$ is the average grey-level of just the right side of the similarly orientated neighbourhood, $N_L(i,j)$ is the average grey-level of just the left side of the similarly orientated neighbourhood and $N_B(i,j)$ is the median value of a large neighbourhood (not orientated). The operator parameters of length and width remained unchanged, the size of the large neighbourhood was set to 151 x 151 pixels. An empirically derived threshold, T2, was applied to all 3 modified line strength measures and followed by the logical AND operator to define the pixel as a vessel.
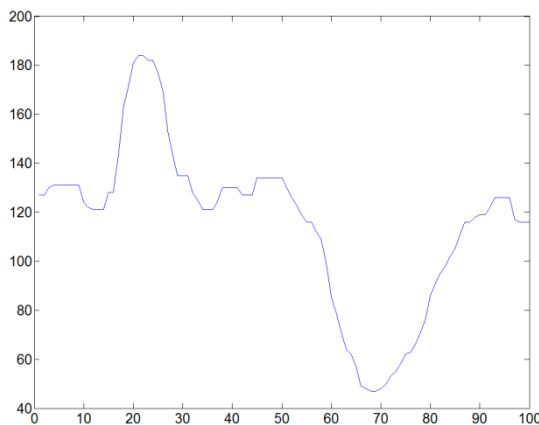
Figure 7: Cross section of a vessel and a bright lesion.

To simplify the explanation of the modifications, figure 7 shows a 1D cross section of a vessel (left of the trace) and a bright lesion (right of the trace) from a pre-processed image. The thresholding of the line strength done in the standard line operator approach was simply stating that $L(i,j)$ must be a value T1 greater than the grey-level average of the similarly orientated neighbourhood. Looking at the trace it's clear that the vessel points are significantly greater than its local neighbourhood. Unfortunately, this is also this case for the edges of the bright lesion due to the large dip in value caused by the bright lesion. This was

the cause of the false responses from the standard approach. The trace shows the difference between the two cases is that vessels are significantly greater than local neighbourhood on both sides unlike non-vessel edges. The first modification was that now $L(i,j)$ was required to be a value of T2 greater than the grey-level average of both the right and the left side of the similarly orientated neighbourhood, which rectified this problem. However, consider two bright lesions in close proximity. The space in-between them is significantly greater than both sides. We could distinguish this case by the fact the pixel value of these points are likely to be similar to that of the retinal background. The median value of a large neighbourhood was used to calculate the retinal background value. Therefore the next modification was that the $L(i,j)$ was required to be a value of T2 greater than the local retinal background value.

The binary vessel maps generated by the modified line operator approach are shown in figure 8. The false responses caused by non-vessel edges were now significantly reduced to the extent that non vessel edges were distinguishable to new vessels. Unfortunately the segmentation of new vessel had become slightly damaged. This is a trait of all vessel segmentation techniques, the more emphasis put on the reduction of non-vessel responses the greater the risk of damage to the segmentation of the vessels. This meant that new vessels were no longer so distinguishable to the normal vasculature.
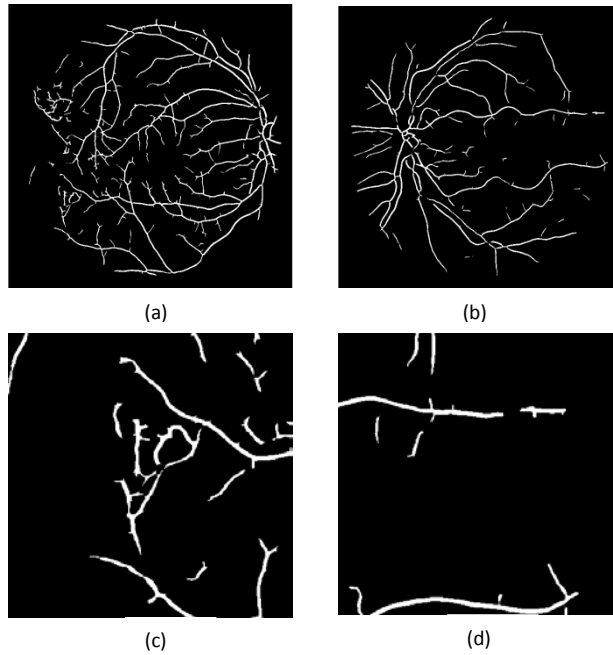
Figure 8: Binary vessel maps corresponding to the images in figure 1, modified line operator.

Both of the segmentation methods showed disadvantages and therefore neither method alone was suitable for the detection of new vessels. However, each of the produced binary maps held vital information. The standard approach provided the information to distinguish new vessel from normal vasculature and the modified approach provided information to distinguish new vessels from non-vessel edges. Extraction of information from both maps could be used effectively to detect new vessels, therefore both segmentation methods were applied.

The segmented results shown in the figures so far also included an additional step to remove any falsely detected microaneurysms and haemorrhages, known as dark lesions. The line operator parameters and the low threshold that were selected to ensure increased sensitivity to new vessels also caused an increased sensitivity to red lesions. A simple measure of circularity (see equation 5) and area from the objects in the binary vessel map was used to distinguish dark lesions and other spurious objects in order to remove them.

$$\text{Circularity} = 4\pi.\text{area}/\text{perimeter}^2 \qquad (5)$$

2.3 Straight Vessel Removal:

Many sections of the normal vasculature possess high local densities, which occur at or near the optic disc, at bifurcation points and at crossover points. Therefore the claim that new vessels could be distinguished from the normal vasculature was only possible if large sections of the normal vasculature were first removed. This was done using a technique proposed by [42], which involves the segmentation of the straight vessels. The standard line operator was applied as before, however the operator length was increased to 81 pixels. The operator was no longer sensitive to the tortuous vessels and was instead only sensitive to relatively straight vessels. An empirically derived threshold, T3, was applied and the resultant straight vessel maps are shown figure 9.

(a)   (b)
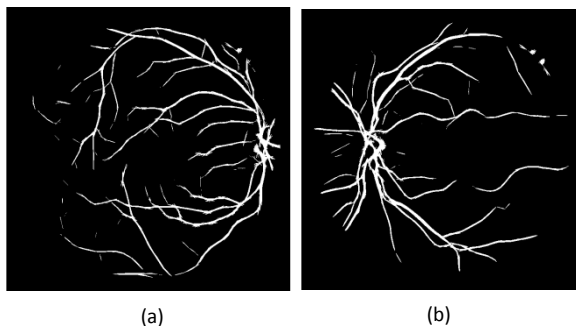
Figure 9: Straight vessel maps corresponding to the images in figure 1.

The binary vessel maps from the standard and modified approach were both skeletonised by means of morphological thinning, to ensure they were thinner than the straight vessel map. Following this the straight vessel map was subtracted from each. The following sections will describe how the binary vessel maps, which now contained only partial vasculature, were assessed for new vessels.

2.4 Feature Extraction:

The design of this method is aimed at the classification of image regions that contain new vessels. These image regions can be described as containing many vessel segments, which are closely spaced, appear in multiple orientations and possess a tortuous nature. There was no intention in this work to identify individual new vessel pixels or segments. Achieving a high performance at such a level of accuracy is currently unrealistic, and even a human observer would struggle due to the often obscure appearance of new vessels.

The binary vessel maps were converted into vessel segments prior to measurements of features. The vasculature was a single pixel in thickness as skeletonization had been performed in the previous stage. Vessel segments were created by removing bifurcation points which were pixels with more than two eight-way neighbours. Finally, small segments consisting of fewer than ten pixels were discarded.

A sub window of size 151 x 151 pixels was created in order to calculate local features associated with the morphology of the vasculature. This sub window was scanned through the image and at each pixel position the four features listed below were calculated. This same set of features was measured from the binary vessel map from each the standard and modified approach to produce two separate feature sets.

1) Number of vessel pixels

2) Number of vessel segments

3) Number of vessel orientations

4) Vessel density

For the third feature, the end points of a segment were connected by a straight line. The angle the line made with the x-axis that fell within the range -90° to 90° of the unit circle was calculated. The calculated angle was accordingly dropped into one of eight bins, each representing a range of angles. This was done for each segment within the sub window and the number of non-empty bins represented the number of orientations. For the fourth feature, a segment was dilated with a disk structuring element with a radius of 20 pixels. The number of vessel pixels within the dilated area was divided by the number of pixels within the segment to give its vessel density. This was done for each segment within the sub window and the mean vessel density was calculated.

2.5 Dual Classification:

The conventional approach for classification is an individual classifier that uses a single feature set. Combining multiple classifiers can enhance the performance of the individual classifier. Fraz [28] described a multiple classifier approach using bagging and boosting techniques, this used a single feature set. Of more relevance to this work are the multiple classifier approaches that use multiple feature sets. Chim [51] proposed a dual classification system that used two different feature sets. The features could have been combined to produce a single feature set, however to achieve a better performance they were kept separate and independent classification was performed which were then combined to produce a final decision.

The proposed methodology adopted a dual classification approach. All features were normalised so that each feature had zero mean and unit standard deviation. Independent classification was performed for each feature set using a support vector machine (SVM) classifier [52,53]. The linear and nonlinear SVMs were tested. The former was used as the latter did not demonstrate any improvements in this application. Each classifier independently

labelled the candidate pixel as new vessels or non-new vessels. The system produced a final decision by combining the outcomes. The candidate pixel achieved a new vessel label only when both classifications agreed on its identity being new vessels, otherwise it achieved a non-new vessel label. When complete, all pixels labelled as new vessels were dilated with a structuring element the size of the sub window to illustrate the new vessel regions.

Whilst only two classes were used, new vessels and non new vessels, both feature sets and their independent classification were not intended to distinguish the same two cases. Classifier 1, associated with the feature set measured from the standard line operator approach, was intended to distinguish new vessels from normal vessels. Classifier 2, associated with the feature set measured from the modified line operator approach, was intended to distinguish new vessels from exudates. Combining the outcomes then removed the false new vessel responses that each classifier made.

3 EXPERIMENTAL EVALUATION:

3.1 Materials:

Due to the low prevalence of new vessel in the screening population, the proposed method was evaluated using images collected from two sources. These were the publicly available MESSIDOR retinal image database, provided by the Messidor program partners [54], and the St Thomas' hospital ophthalmology department. A total of 60 images were included in the dataset: 20 with confirmed new vessels and a further 40 images without new vessels. The image data from each source were as follows:

1) MESSIDOR: 5 new vessel images, 20 normal images and 20 images with the large majority showing other DR pathology (mainly bright lesions) and the remainder

showing strong reflection artefacts. These images were acquired from a colour video 3CCD camera on a Topcon TRC NW6 fundus camera with a 45 degree field of view (FOV) and an image resolution of 2240 x 1488 pixels.

2) St Thomas' Hospital: 15 new vessel images acquired with a Nikon D80 digital SLR camera on a Topcon TRC NW6 fundus camera with a 45 degree FOV and an image resolution of 2896 x 1944 pixels. Ethical approval was obtained for the use of these images.

Images were scaled to the same size using a spatial normalization technique proposed by [55] along with bicubic interpolation and anti-aliasing. This was based on normalizing the FOV width, with the requirement that all images were captured with the same FOV angle. All images were normalized to have a FOV width of 1379 pixels. This was followed by cropping to remove some of the surrounding black boarder to produce images of size 1479 x 1479 pixels.

For training data, image patches the same size of the sub window were created from the dataset and each was labelled as either new vessels or non-new vessels by an ophthalmologist. Separate training data was used for each classifier. Classifier 1 was trained with 50 new vessel patches and 50 normal vessel patches. Classifier 2 was trained with 50 new vessel patches and 50 patches made up of a variety of bright lesions, dark lesions and reflection artefacts. Testing was performed across the whole of each retinal image, in terms of the classification process being performed at every pixel location. Because of the limited size of the dataset, splitting the data set to create separate training and testing sets was not suitable. Instead, both the training and testing sets were created using the same selection of images (entire dataset). Evaluation in this manner would clearly cause over fitting of the model, therefore the leave-one-out cross validation method was applied. This meant the classifiers were trained using all the patches from all the images except those from the single test image, and this process was

repeated for each image. The feature value normalization was also recalculated each time, leaving out the test image.

As mentioned above, the system made decisions on a pixel basis. As stated previously features were extracted using information from the local neighbourhood contained within the sub window centred over the target pixel. Positive pixels were then dilated by the size of the sub window to delineate the new vessels regions. However, the performance from a per image basis is more useful from a clinical point of view. An image simply achieved a new vessel label if it contained any delineated regions. Prior to this, all images had been labelled by an ophthalmologist using the same labels as before but on a per image basis.

To get a more detailed insight into the system's performance, evaluation was also performed on a per patch basis. The logical approach was to perform testing on the training patches using the leave-one-out cross validation method. This was followed, except many more patches were created and labelled by an ophthalmologist to increase the testing data.

3.2 Performance Measures:

It is common practice to evaluate the performance of such machine learning algorithms using the receiver operating characteristic (ROC) curve. This was created by plotting the true positive rate (sensitivity) versus the false positive rate (1-specificity) at various threshold levels of the probability score of the classifier. The SVM estimated a new vessel probability score using the distance to the decision boundary. However due to the dual classifier approach and therefore two probability scores, the creation of ROC curves was not a straight-forward task.

This problem was tackled by creating a 3D ROC surface. The majority of literature relating to higher dimensional ROC analysis relates to multi-class analysis [56,57] and are of little relevance. Of more relevance are studies that add a third dimension by varying the threshold

of an additional parameter [58]. To our knowledge, there appears to be no available literature concerning ROC analysis for dual classifiers.
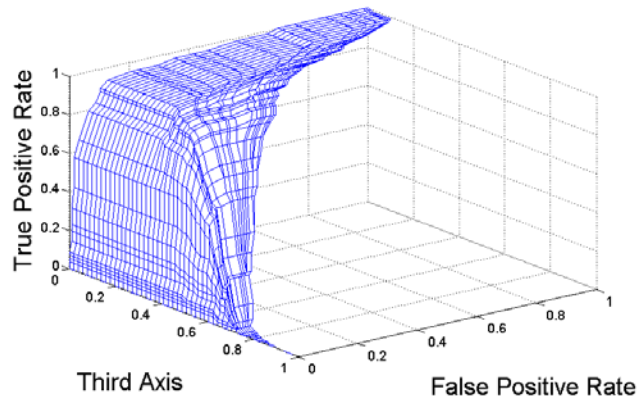
Figure 10: 3D ROC surface for the performance on a per patch basis. The third axis is required to vary the threshold of the probability score of the additional classifier that arises in a dual classification approach.

Mentioned above, a conventional 2D ROC curve has 2 axes and the points of the curve are created by varying the threshold of the probability score of the classifier. In this scenario, consider the thresholding in concern was that of the probability score of classifier 2. The addition of a third axis was used to represent the thresholding of the probability score of classifier 1. The resultant was a 3D ROC surface that explores all combinations of thresholds for the dual classification. Figure 10 shows the 3D ROC surface representing performance on a per patch basis.

Information from this 3D ROC surface was extracted to create a 2D ROC curve. For each false positive rate value its maximum true positive rate value was found by searching along the third axis. From this 2D plot the area under the curve (AUC) was extracted and used as a performance measure.

Theoretically, plotting the points for all combinations of thresholds of the two probability scores directly on a 2D coordinate system was a viable option. However, the use of a 3D ROC

surface provided better visualization in respect to how varying the threshold for each of the probability scores affected the performance.

3.3 Results:

The ROC curves for evaluation on a per patch basis and per image basis are depicted in figures 11 and 12. The AUC value for the per patch basis is 0.9632. A maximum accuracy is achieved at an operating point giving a sensitivity (SN) of 0.8793 and a specificity (SP) of 0.9440. An alternate operating point gives a sensitivity of 0.9137 and a specificity of 0.9200. For the per image basis the AUC value is 0.9682. The operating point with maximum accuracy gives a sensitivity of 1.00 and a specificity of 0.90. The performance from a per image basis is more useful from a clinical point of view. Examples of classified images are given in figure 13. Classified new vessel regions have also been indicated with a white boundary. Images containing any delineated regions are classified as new vessel images. Table 1 shows these results along with the reported results from other new vessel detection methods. The MATLAB Code took 450 seconds on an Intel(R) core(TM)2 Quad CPU Q9300 at 2.5 GHz to process each image.
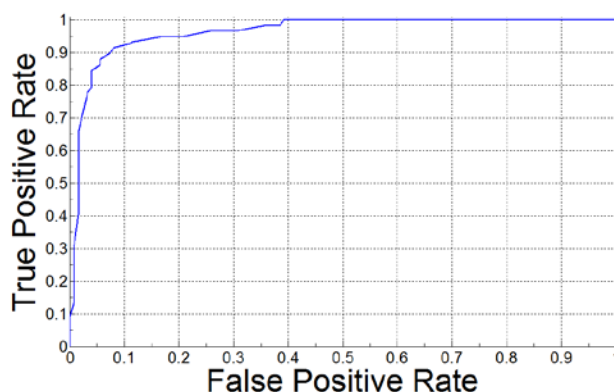
Figure 11: ROC curve for the performance on a per patch basis.
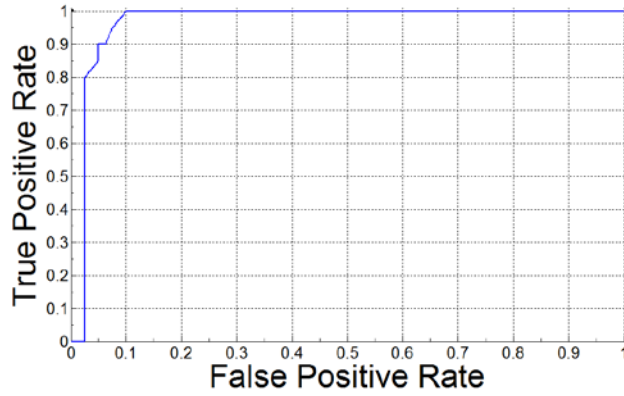
Figure 12: ROC curve for the performance on a per image basis.

Methods	AUC	SN	SP	Level
Jelinek [38]	0.9000	0.9400	0.8200	Image
Goatman [39]	0.9110	0.8420	0.8590	Image
Akram [40]	-	0.9893	0.9635	Segment
Hassan [41]	0.7045	0.6390	0.8940	Pixel
Agurto [46]	0.9400	0.9600	0.8300	Image
Welikala [42]	-	1.0000	0.7000	Image
Proposed	0.9632	0.8793	0.9440	Patch
Proposed	0.9682	1.0000	0.9000	Image

Table 1: Reported results for new vessel detection methods.
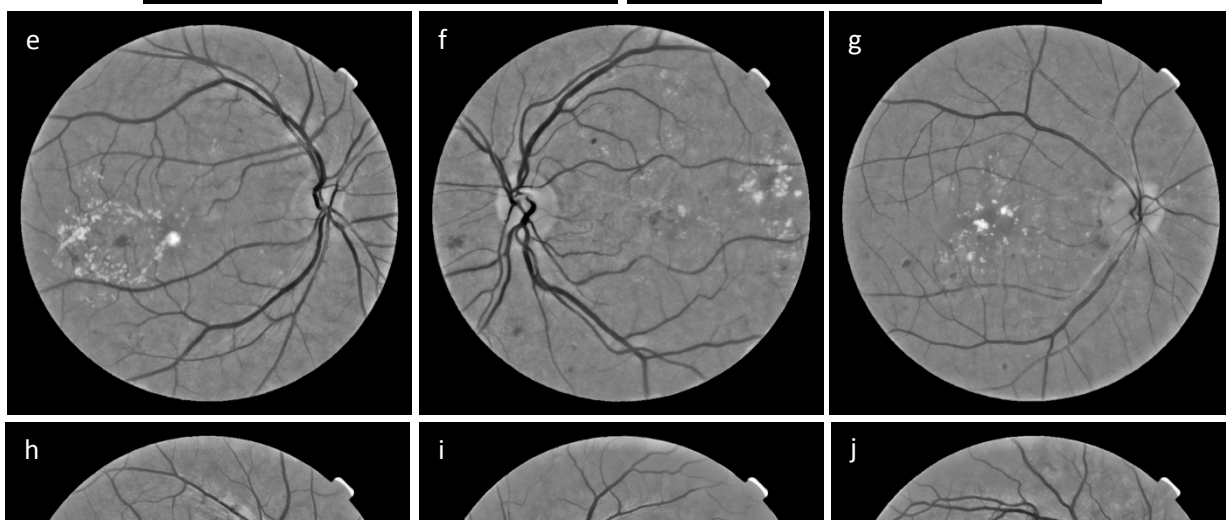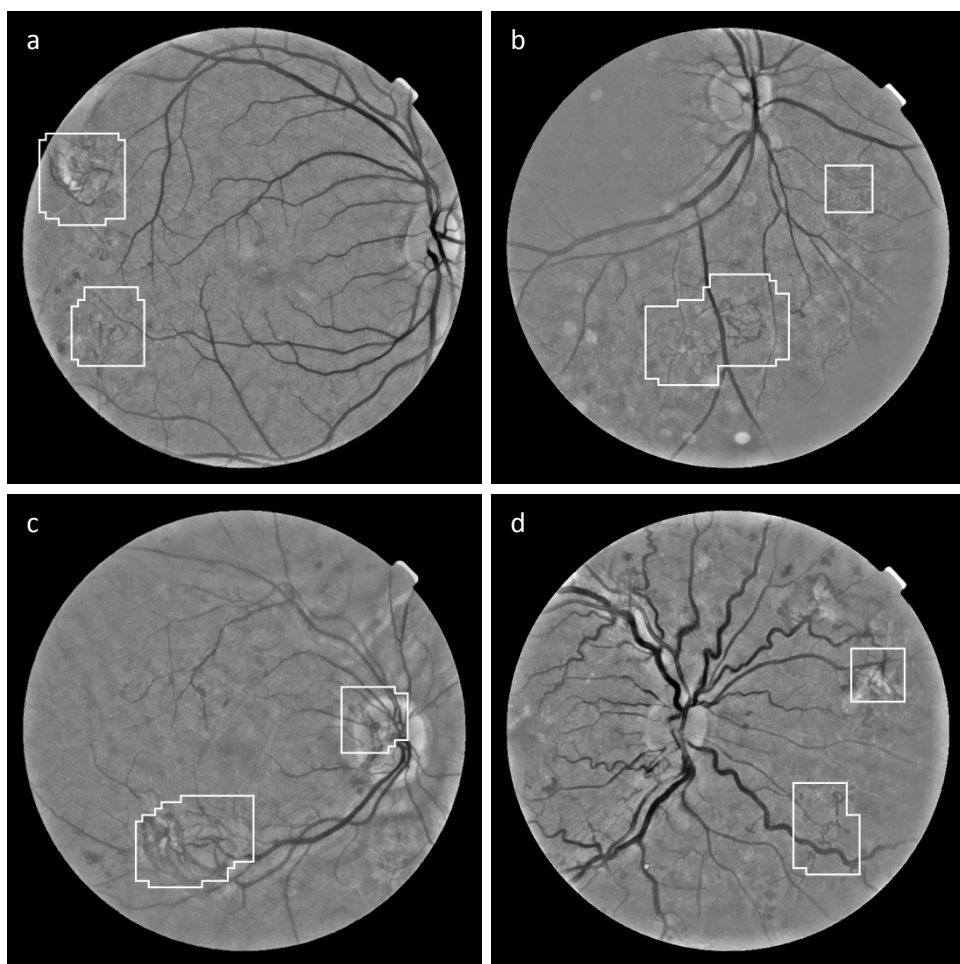
Figure 13: Results of the algorithm applied to the dataset. (a)-(d) True positive images, (e)-(i) true negative images, (j) false positive image.
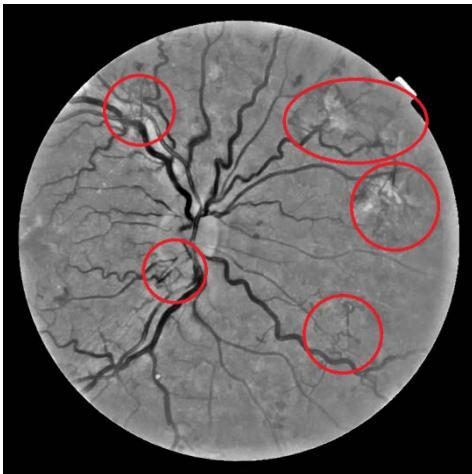
Figure 14: Manual delineation of new vessel regions by an ophthalmologist.

4 DISCUSSION AND CONCLUSION:

In this paper, we have presented an effective new vessel detection method based on a dual classification approach and a four dimensional feature vector used to analyse the morphology of the local retinal vasculature.

The main contribution of this paper is the novel application of a dual classification approach to independently process two different segmented vessel maps with the objective to detect new vessels whilst reducing false responses caused by bright lesions and other retinal features. Segmentation methods include the standard line operator and a novel modified line operator. The latter targets the reduction of false responses to non-vessel edges. In addition, emphasis is put on ensuring new vessels are adequately segmented with the correct selection of parameters for vessel segmentation. Another important point emphasised in this paper, is that high vessel area alone is not enough to identify new vessels. A more detailed analysis of the morphology of the vasculature is required as well as the removal of straight vessels.

From the examples of classified images shown in figure 13 it is evident that the algorithm responds well to a variety of new vessel formations. This includes both new vessels elsewhere (NVE) and new vessels at the optic disc (NVD), new vessels with associated fibrosis and obscure new vessels. Also evident is the algorithm's ability to avoid false responses despite the presence of bright lesions, dark lesions and reflection artefacts. Figure 13(j) shows a false positive image caused by vessels from the layer beneath the retina (choroid) being visible. This is an unusual case because when vessels from this layer are visible they normally possess little contrast to the background and often have a wider calibre, therefore they do not get segmented. Another cause of false responses are dilated capillaries known as intra-retinal microvascular abnormalities (IRMA) which are very difficult to differentiate from new vessels. IRMA represents a stage of DR that indicates a high risk of the progression of new vessels. A final area of evident difficultly to the algorithm concerns the spacing between bright lesions of close proximity. On rare occasions these areas appear significantly darker than the retinal background and therefore the modified line operator can fail to avoid their segmentation.

In 2002, studies from the UK [59,60] reported the prevalence of PDR is 3.7% for patients with type 1 diabetes and 0.5% for patients with type 2 diabetes. When taking into the account the

proportions of patients with each type of diabetes in the UK, an overall value of 0.82% can be derived. Although the prevalence of PDR is low, the associated risk of the rapid onset of vision loss means it must be detected reliably. In UK screening programmes it is considered a serious breach in protocol if an image with PDR is either missed or delayed in referral. Therefore the maximum sensitivity of 1.00 that our algorithm reaches on a per image basis whilst achieving a respectable specificity of 0.90 gives it potential for clinical application. However, when considering the low prevalence of PDR, this specificity value is lacking. The results indicate if the algorithm is applied in screening programmes that for every correctly identified patient with PDR there would be approximately 12 incorrectly identified patients. This calculation does not consider that the 40 non new vessel images from the dataset used to calculate specificity were chosen to make this dataset more challenging and is therefore not a true representative of a screening population. This calculation also does not take into consideration that on average 4 images are obtained for each patient. A final point not considered in this calculation is that a proportion of patients with PDR will already be under the care of ophthalmology and therefore are not required to attend screening.

The proposed method does achieve better performance metrics than the other published methods, as shown in table 1. However, true comparisons are difficult to make as no standard datasets have been used for testing. Also from the small handful of published results, there exists variability in terms of their application. Goatman [39] and Agurto [46] seek to only detect new vessels at the optic disc. Jelinek [38] applied their methods on fluorescein images, which have the advantage of possessing a very high vessel to background contrast. However, image capture using fluorescein is an invasive procedure and therefore is not suitable for the large scale screening programmes.

Our algorithm's SN and SP results that achieve the maximum accuracy on each level (image and patch) do not correspond to the same operating point. The reported per image

performance of 1.00 and 0.90 for SN and SP respectively corresponds to a per patch performance of 0.5172 and 0.9840 for SN and SP respectively. This shows, for this per image performance, that the system puts no emphasis on detecting and correctly delineating all new vessels. Instead identifying any part of any new vessels in the image is sufficient to achieve a positive image label. Figure 13(d) illustrates how there is no requirement to identify all new vessels in the image, with only two out of the five new vessel networks being identified. Figure 14 shows the location of all five new vessel networks. Such an approach assists in obtaining a higher specificity whilst being careful to ensure the maximum sensitivity is still retained. Niemeijer [13] follows this same approach but in respect to dark lesion detection. Such an approach may hold certain risks, although it is still a viable option for clinical application.

Previously mentioned were other vessel segmentation methods [33,34] that specialize in the reduction of false responses caused by bright lesions. However, the reduction has to achieve a more comprehensive level if they are to be successfully applied in PDR detection. Our modified line operator achieves such required levels, particularly due to the additional step taken to resolve the false response caused by the space in-between bright lesions of close proximity. Such a comprehensive level inevitably risks damage to the segmented vessels and therefore brought around the requirement of a dual system.

Future developments of this method will include the evaluation of new vessel delineation. Whilst the accurate delineation of new vessels regions was not an objective of this method, its performance evaluation provides a comprehensive approach in respect to gaining a detailed insight into the system's performance. This will provide additional detail to that gained by the evaluation on a per patch basis. Requirements are the careful manual delineation of new vessel regions by an ophthalmologist to create ground truth images. Further development concerning the vessel segmentation approaches shall be explored. Currently a global threshold is applied, although a more sophisticated approach such as adaptive thresholding or

a supervised machine learning approach may yield better results. Another intended development involves the extraction of further information regarding the morphology of the vasculature in order create a higher dimensional feature set. A mean tortuosity measure had been calculated by dividing the true length by Euclidean length for each segment in the sub window followed by averaging. However, it was excluded from the feature set as it reduced the system's performance. Such an important new vessel characteristic has to be calculated more effectively and reassessed.

All existing PDR detection methods define new vessels as dense lacy networks of unregulated vessel growth. This description does not match their appearance at their initial formation, when they can appear as loops or small networks. These changes in the vasculature can be so subtle and it is likely that all existing methods, including our work, would fail in detecting such cases. These cases must still receive urgent referral to a specialist, although they possess far less risk of a rapid onset of vision reduction in comparison to large regions of abnormal vessel growth. Another difficultly of PDR detection is caused by retinal features associated with new vessels which may on occasion obscure or completely hide them from view. This includes pre-retinal and vitreous haemorrhages caused by the rapture of new vessels and tractional retinal detachment caused by fibrosis. On the positive side such cases are clearly identifiable and therefore can be flagged up by the photographer performing the screening test.

Our methodology was not solely tested on images from publicly available data sets due to their limited inclusion of new vessel images. To assist in the development of PDR detection algorithms it is vital that a large new vessel data set becomes publicly available. New vessel formations can vary greatly in appearance, thus this should be represented in the data set. With a standard data set, comparisons of published methods will be possible.

In conclusion, this paper has demonstrated an automated system that is capable of detecting the presence of new vessels whilst reducing false responses to bright lesions and other retinal

features. The proposal of introducing automated disease/no disease systems into DR screening programmes to reduce the manual grading workload have been considered. The addition of PDR detection will greatly strengthen the proposal by ensuring images requiring urgent referrals are automatically prioritized.

5 REFERENCES:

[1] P.M. Dodson, Oxford Diabetes Library: Diabetic Retinopathy, Oxford University Press (2008).

[2] I. Kocur and S. Resnikoff, Visual impairment and blindness in europe and their prevention, British Journal of Ophthalmology 86 (2002) 716.

[3] H.R. Taylor and J.E. Keeffe, World blindness: a 21st century perspective, British Journal of Ophthalmology 85 (2001) 261-266.

[4] S. Wild, G. Roglic, A. Green, R. Sicree, H. King, Global prevalence of diabetes: estimates for the year 2000 and projections for 2030. Diabetes Care 27 (2004) 1047-1053.

[5] T. Bek and M. Erlandsen, Visual prognosis after panretinal photocoagulation for proliferative diabetic retinopathy. Acta Ophthalmologica Scandinavica 84 (2006) 16.

[6] J.P. De La Cruz, J.A. Gonzalez-Correa, A. Guerrero, Pharmacological approach to diabetic retinopathy, Diabetes/metabolism research and reviews 20 (2004) 91-113.

[7] U.K National Screening Committee, Essentials Elements in Developing a Diabetic Screening Programme. Workbook Version 4.3, (2009).

[8] D.C. Klonoff and D.M. Schwartz, An economic analysis of interventions for diabetes, Diabetes Care 23 (2000) 390.

[9] R.N. Frank, Diabetic retinopathy, Progress in Retinal and Eye Research 14 (1995) 361-392.

[10] J.J. Kanski and B. Bowling, Clinical Ophthalmology: A Systematic Approach. Seventh edition. Elsevier Limited (2011).

[11] A.D. Fleming, K.A. Goatman, S. Philip, G.J. Prescott, P.F. Sharp, J.A. Olson, Automated grading for diabetic retinopathy: a large-scale audit using arbitration by clinical experts, British Journal of Ophthalmology 94 (2010) 1606-1610.

[12] T. Spencer, J.A. Olson, K.C. McHardy, P.F. Sharp, J.V. Forrester, An image-processing strategy for the segmentation and quantification of microaneurysms in fluorescein angiograms of the ocular fundus, Computers and Biomedical Research 29 (1996) 284-302.

[13] M. Niemeijer, B. van Ginneken, J. Staal, M.S.A. Suttorp-Schulten, M.D. Abramoff, Automatic detection of red lesions in digital color fundus photographs, IEEE Transactions on Medical Imaging 24 (2005) 584-592.

[14] A. Sopharak, B. Uyyanonvara, S.A. Barman, Simple hybrid method for fine microaneurysm detection from non-dilated diabetic retinopathy retinal images, Computerized Medical Imaging and Graphics (2013).

[15] L. Tang, M. Niemeijer, J.M. Reinhardt, M.K. Garvin, M.D. Abramoff, Splat feature classification with application to retinal hemorrhage detection in fundus images, IEEE Transactions on Medical Imaging 32 (2013) 364-375.

[16] M.D. Saleh and C. Eswaran, An automated decision- support system for non- proliferative diabetic retinopathy disease based on MAs and HAs detection, Computer methods and programs in biomedicine 108 (2012) 186-196.

[17] T. Walter, J. Klein, P. Massin, A. Erginay, A contribution of image processing to the diagnosis of diabetic retinopathy-detection of exudates in color fundus images of the human retina, IEEE Transactions on Medical Imaging 21 (2002) 1236-1243.

[18] A. Sopharak, B. Uyyanonvara, S.A. Barman, Automatic exudate detection from non-dilated diabetic retinopathy retinal images using fuzzy C-means clustering, Sensors 9 (2009) 2148-2161.

[19] A. Sopharak, M.N. Dailey, B. Uyyanonvara, S.A. Barman, T. Williamson, K.T. Nwe, et al., Machine learning approach to automatic exudate detection in retinal images from diabetic patients, Journal of Modern Optics 57 (2010) 124-135.

[20] A. Osareh, M. Mirmehdi, B. Thomas, R. Markham, Automated identification of diabetic retinal exudates in digital colour images, British Journal of Ophthalmology 87 (2003) 1220-1223.

[21] D. Youssef and N.H. Solouma, Accurate detection of blood vessels improves the detection of exudates in color fundus images, Computer methods and programs in biomedicine 108 (2012) 1052-1061.

[22] S. Chaudhuri, S. Chatterjee, N. Katz, M. Nelson, M. Goldbaum, Detection of blood vessels in retinal images using two-dimensional matched filters, IEEE Transactions on Medical Imaging 8 (1989) 263-269.

[23] A.M. Mendonca and A. Campilho, Segmentation of retinal blood vessels by combining the detection of centerlines and morphological reconstruction, IEEE Transactions on Medical Imaging 25 (2006) 1200-1213.

[24] G.B. Kande, P.V. Subbaiah, T.S. Savithri, Unsupervised fuzzy based vessel segmentation in pathological digital fundus images, Journal of Medical Systems 34 (2010) 849-858.

[25] J. Staal, M.D. Abramoff, M. Niemeijer, M.A. Viergever, B. van Ginneken, Ridge-based vessel segmentation in color images of the retina, IEEE Transactions on Medical Imaging 23 (2004) 501-509.

[26] J.V.B. Soares, J.J.G. Leandro, R.M. Cesar Jr, H.F. Jelinek, M.J. Cree, Retinal vessel segmentation using the 2-D Gabor wavelet and supervised classification, IEEE Transactions on Medical Imaging 25 (2006) 1214-1222.

[27] E. Ricci and R. Perfetti, Retinal blood vessel segmentation using line operators and support vector classification, IEEE Transactions on Medical Imaging 26 (2007) 1357-1365.

[28] M.M. Fraz, P. Remagnino, A. Hoppe, B. Uyyanonvara, A.R. Rudnicka, C.G. Owen, et al., An ensemble classification based approach applied to retinal blood vessel segmentation, IEEE Transactions on Biomedical Engineering 59 (2012) 2538-2548.

[29] D. Marín, A. Aquino, M.E. Gegúndez-Arias, J.M. Bravo, A new supervised method for blood vessel segmentation in retinal images by using gray-level and moment invariants-based features, IEEE Transactions on Medical Imaging 30 (2011) 146-158.

[30] M. Saez, S. Gonzalez-Vazquez, M. Gonzalez-Penedo, M.A. Barcelo, M. Pena-Seijo, G.C. de Tuero, et al., Development of an automated system to classify retinal vessels into arteries and veins, Computer methods and programs in biomedicine 108 (2012) 367-376.

[31] A. Bhuiyan, R. Kawasaki, E. Lamoureux, K. Ramamohanarao, T.Y. Wong, Retinal artery–vein caliber grading using color fundus imaging, Computer methods and programs in biomedicine 111 (2013) 104-114.

[32] M.M. Fraz, P. Remagnino, A. Hoppe, B. Uyyanonvara, A.R. Rudnicka, C.G. Owen, et al., Blood vessel segmentation methodologies in retinal images - A survey, Computer methods and programs in biomedicine 108 (2012) 407-433.

[33] L. Zhang, Q. Li, J. You, D. Zhang, A modified matched filter with double-sided thresholding for screening proliferative diabetic retinopathy, IEEE Transactions on Information Technology in Biomedicine 13 (2009) 528-534.

[34] B. Zhang, L. Zhang, L. Zhang, F. Karray, Retinal vessel extraction by matched filter with first-order derivative of Gaussian, Computers in Biology and Medicine 40 (2010) 438-445.

[35] G.S. Ramlugun, V.K. Nagarajan, C. Chakraborty, Small retinal vessels extraction towards proliferative diabetic retinopathy screening, Expert Systems with Applications 39 (2012) 1141-1146.

[36] A. Daxer, Characterisation of the neovascularisation process in diabetic retinopathy by means of fractal geometry: diagnostic implications, Graefe's archive for clinical and experimental ophthalmology 231 (1993) 681-686.

[37] A. Karperien, H.F. Jelinek, J.J.G. Leandro, J.V.B. Soares, R.M. Cesar Jr, A. Luckie, Automated detection of proliferative retinopathy in clinical practice, Clinical Ophthalmology 2008 (2008) 109.

[38] H.F. Jelinek, M.J. Cree, J.J. Leandro, J.V. Soares, R.M. Cesar Jr, A. Luckie, Automated segmentation of retinal blood vessels and identification of proliferative diabetic retinopathy, Journal of the Optical Society of America.A, Optics, image science, and vision 24 (2007) 1448-1456.

[39] K.A. Goatman, A.D. Fleming, S. Philip, G.J. Williams, J.A. Olson, P.F. Sharp, Detection of new vessels on the optic disc using retinal photographs, IEEE Transactions on Medical Imaging 30 (2011) 972.

[40] M.U. Akram, A. Tariq, S.A. Khan, Detection of neovascularization for screening of proliferative diabetic retinopathy, In Proceedings of the 9th international conference on Image Analysis and Recognition - Volume Part II (2012) 372-379.

[41] S.S.A. Hassan, D.B.L. Bong, M. Premsenthil, Detection of neovascularization in diabetic retinopathy, Journal of digital imaging : the official journal of the Society for Computer Applications in Radiology (2011).

[42] R.A. Welikala, V. Tah, T.H. Williamson, A. Hoppe, J. Dehmeshki, S.A. Barman, Differing matched filter responsivity for the detection of proliferative diabetic retinopathy, Proceedings of the IASTED International Conference Signal Processing, Pattern Recognition and Applications (2013) 356-364.

[43] A.J. Frame, P.E. Undrill, J.A. Olson, K.C. McHardy, P.F. Sharp, J.V. Forrester, Texture analysis of retinal neovascularisation, IEE Colloquium on Pattern Recognition (Digest No. 1997/018) (1997) 5/1-5/6.

[44] U.R. Acharya, E.Y.K. Ng, J. Tan, S.S. Vinitha, K. Ng, An integrated index for the identification of diabetic retinopathy stages using texture parameters, Journal of Medical Systems 36 (2012) 2011-2020.

[45] C. Agurto, V. Murray, E. Barriga, S. Murillo, M. Pattichis, H. Davis, et al., Multiscale AM-FM methods for diabetic retinopathy lesion detection, IEEE Transactions on Medical Imaging 29 (2010) 502-512.

[46] C. Agurto, Y. Honggang, V. Murray, M.S. Pattichis, S. Barriga, W. Bauman, et al., Detection of neovascularization in the optic disc using an AM-FM representation, granulometry, and vessel segmentation, Annual International Conference of the IEEE, Engineering in Medicine and Biology Society (EMBC) (2012) 4946-4949.

[47] K. Zutis, E. Trucco, J.P. Hubschman, D. Reed, S. Shah, J. van Hemert, Towards automatic detection of abnormal retinal capillaries in ultra-widefield-of-view retinal angiographic exams, International Conference on Engineering in Medicine and Biology (2013).

[48] C.N. Doukas, I. Maglogiannis, A.A. Chatziioannou, Computer-supported angiogenesis quantification using image analysis and statistical averaging, IEEE Transactions on Information Technology in Biomedicine 12 (2008) 650-657.

[49] S.M. Pizer, E.P. Amburn, J.D. Austin, R. Cromartie, A. Geselowitz, T. Greer, et al., Adaptive histogram equalization and its variations, Computer vision, graphics, and image processing 39 (1987) 355-368.

[50] R. Zwiggelaar, S.M. Astley, C.R.M. Boggis, C.J. Taylor, Linear structures in mammographic images: detection and classification, IEEE Transactions on Medical Imaging 23 (2004) 1077-1086.

[51] Y.-. Chim, A.A. Kassim, Y. Ibrahim, Dual classifier system for handprinted alphanumeric character recognition, Pattern Analysis and Applications 1 (1998) 155-162.

[52] B.E. Boser, I.M. Guyon, V.N. Vapnik, A training algorithm for optimal margin classifiers, Proceedings of the fifth annual workshop on Computational learning theory (1992) 144-152.

[53] N. Cristianini and J. Shawe-Taylor, An introduction to support vector machines and other kernel-based learning methods, Cambridge university press (2000).

[54] MESSIDOR, 2004.

[55] X. Zhang, G. Thibault, E. Decencière, G. Quellec, G. Cazuguel, A. Erginay, et al., Spatial normalization of eye fundus images, IEEE International Symposium on Biomedical Imaging (2012).

[56] T. Landgrebe and R. Duin, A simplified extension of the area under the ROC to the multiclass domain, Seventeenth annual symposium of the pattern recognition association of South Africa (2006).

[57] M.S. Wandishin and S.J. Mullen, Multiclass ROC analysis, Weather and Forecasting 24 (2009) 530-547.

[58] D.L. Simon, A three-dimensional receiver operator characteristic surface diagnostic metric, Annual Conference of the Prognostics and Health Management Society (2010).

[59] N. Younis, D.M. Broadbent, S.P. Harding, J.P. Vora, Incidence of sight-threatening retinopathy in Type 1 diabetes in a systematic screening programme, Diabetic Medicine 20 (2003) 758-765.

[60] N. Younis, D.M. Broadbent, J.P. Vora, S.P. Harding, Incidence of sight-threatening retinopathy in patients with type 2 diabetes in the Liverpool Diabetic Eye Study: a cohort study, The Lancet 361 (2003) 195-200.